14

Photovoltaic/Wind Energy System with Hydrogen Storage

Mamadou Lamine Doumbia and Kodjo Agbossou
Hydrogen Research Institute
Department of Electrical and Computer Engineering
Université du Québec à Trois-Rivières
C.P. 500, Trois-Rivières (Québec) G9A 5H7
Canada

1. Introduction

Renewable energy systems (RES) such as photovoltaic and wind generators are increasingly used as a means to satisfy the growing need for electric energy around the world. For many years, the Hydrogen Research Institute (HRI) has developed a renewable photovoltaic/wind energy system based on hydrogen storage. The system consists of a wind turbine generator (WTG) and a solar photovoltaic (PV) array as primary energy sources, a battery bank, an electrolyzer, a fuel cell stack, different power electronics interfaces for control and voltage adaptation purposes, a measurement and monitoring system. The renewable energy system can operate in stand-alone or grid-connected mode and different control strategies can be developed.

This paper presents the HRI's grid-connected renewable energy system (RES). The system's main components i.e. photovoltaic arrays, wind turbine, batteries, electrolyzer and fuel cell, are described individually and their modelling and simulation methodologies are presented. The complete system model is developed by integrating individual sub-units. Matlab/Simulink and LabVIEW softwares are used for modelling, programming and analyzing the behavior of each system sub-unit. The state of charge control method was used to validate the developed simulation models. The results obtained with the two modelling and simulation softwares were compared. Stand-alone and grid-connected operating conditions are investigated and experimental data are provided to support theoretical and simulation analyses. The power transfer study in the interconnected system is also presented. Such a global model is useful for understanding the system's operation, and optimal dimensioning and effective control of the renewable energy system with hydrogen storage (RESHS) (Kim S-K et al., 2008).

2. System components modelling

Figure 1 shows the block diagram of the HRI renewable energy system (Doumbia et al., 2007). The system consists of a 10 kW permanent magnet wind turbine generator and a 1 kW solar photovoltaic (PV) array as primary energy sources, a battery bank with 48V voltage, a 5 kW electrolyzer, a 1.2 kW proton exchange membrane fuel cell (PEMFC) stack. A 5 kW reversible inverter is used to convert 48V DC bus voltage into alternating current (AC) with 115V. The inverter output can be connected to the utility grid or to power a local AC load. A buck converter is used to control the electrolyzer and a boost converter is used to convert the 24V PEMFC output voltage into 48V DC bus voltage.

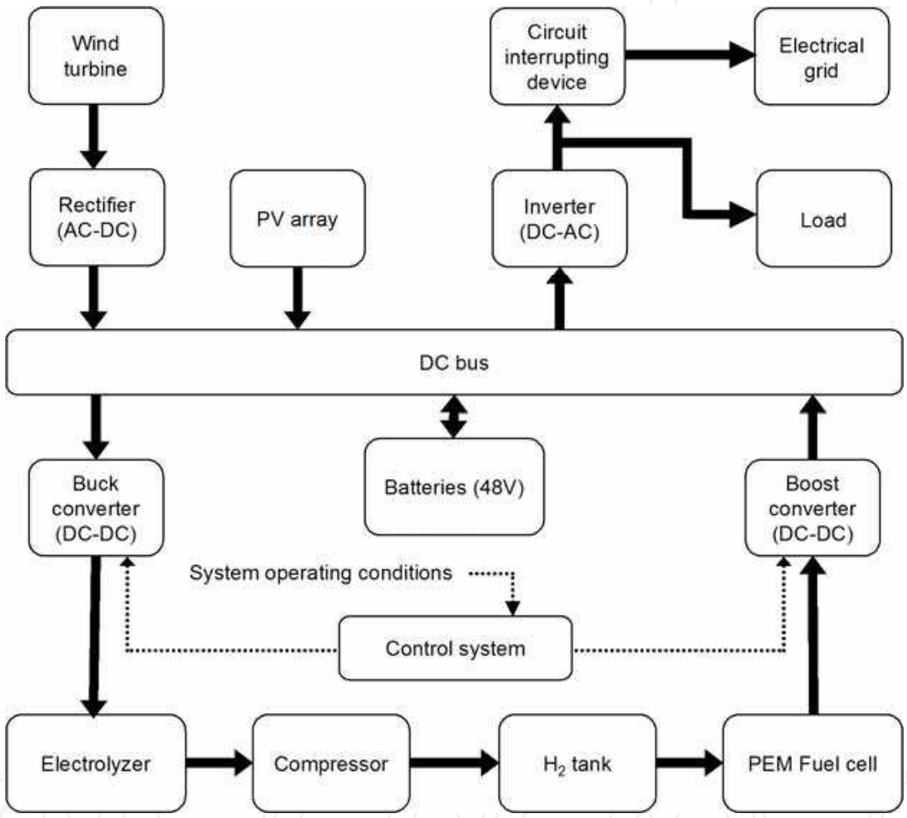

Fig. 1. Block diagram of the HRI's renewable energy system with hydrogen storage

2.1 Photovoltaic Array

The solar array is a group of several modules electrically connected in series-parallel combinations to generate the required current and voltage. The photovoltaic (PV) module output current I is equal to the photo-generated current I_L, less the diode-current I_d and the shunt-leakage current I_{sh}. The series resistance R_s represents the internal resistance to the current flow, and depends on the p-n junction depth, the impurities and the contact resistance. The shunt resistance R_{sh} is inversely related with leakage current to the ground. In an ideal PV cell, $R_s = 0$ (no series loss), and $R_{sh} = \infty$ (no leakage to ground).

In the equivalent circuit, the current delivered to the external load equals the current I_L generated by the illumination, less the diode current I_d and the ground-shunt current I_{sh}. The open circuit voltage V_{oc} of the cell is obtained when the load current is zero, and is given by the equation (1):

$$V_{oc} = V + IR_s \tag{1}$$

The mathematical description of the current-voltage (I-V) characteristic for photovoltaic (PV) cells has been available for some time. The simplest equivalent circuit of a solar cell is a current source in parallel with a diode (Figure 2). The output of the current source is directly proportional to the light falling on the cell. The diode determines the I-V characteristics of the cell (Walker, 2000), (Gow & Manning, 1999). The model includes temperature dependence of the photo-current I_L and the saturation current of the diode I_0.
The equations which describe the I-V characteristics of the cell are:

$$I = I_L - I_0\left(e^{\frac{q(V+IR_S)}{nkT}} - 1\right) \tag{2}$$

where :

I_L = photo-generated current (A)
I_0 = diode saturation current (A)
q = electronic charge (C)
V = solar cell terminal voltage (V)
R_S = cell series resistance (Ω)
n = diode quality factor
k = Boltzmann's constant (J/K)
T = ambient temperature (K)

$$I_L = I_{L(T1)}\left(1 + K_0\left(T - T_1\right)\right) \tag{3}$$

$$I_{L(T1)} = \frac{G * I_{SC(T1)}}{G_{nom}} \tag{4}$$

$$K_0 = \frac{I_{SC(T2)} - I_{SC(T1)}}{I_{SC(T1)}\left(T_2 - T_1\right)} \tag{5}$$

where :
G = cell irradiance (W/m²)
G_{nom} = rated cell irradiance (W/m²)
T = solar cell temperature (K)
T_1, T_2 = two reference temperatures (K)
$I_{SC(T1)}$ = short circuit current at temperature T_1 (A)
$I_{SC(T2)}$ = short circuit current at temperature T_2 (A)

The diode saturation current I_0 can be determined by the equation (6) :

$$I_0 = I_{0(T_1)}\left(\frac{T}{T_1}\right)^{\frac{3}{n}} e^{\frac{-qVg}{nk}\left(\frac{1}{T}-\frac{1}{T_1}\right)} \tag{6}$$

$$I_{0(T_1)} = \frac{I_{SC(T_1)}}{e^{\frac{qVoc(T_1)}{nkT_1}\left(\frac{1}{T}-\frac{1}{T_1}\right)}-1} \tag{7}$$

where:

V_g = Band gap voltage (V)

$V_{OC(T1)}$ = Open circuit voltage at the temperature T_1 (V)

The cell series resistance R_S is

$$R_S = -\frac{dV}{dI_{Voc}} - \frac{1}{X_V} \tag{8}$$

$$X_V = I_{0(T_1)}\frac{q}{nkT_1} e^{\frac{qVoc(T_1)}{nkT_1}} \tag{9}$$

$\frac{dV}{dI_{Voc}}$ is the voltage-current derivative when the voltage has reached open-circuit value.

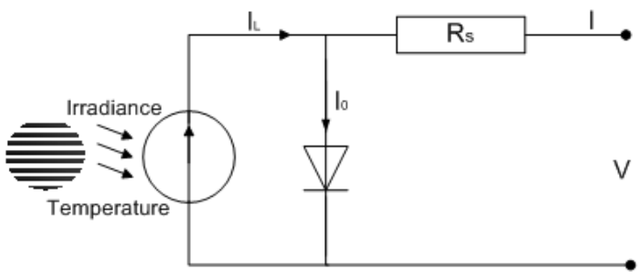

Fig. 2. Circuit diagram of PV model

Solar panels installed at IRH are composed of 16 modules, i.e. four rows of four serial connected modules. The electrical performance and the characteristic curves of the PV modules are dependent on temperature and illumination. From the preview equations, the I-V characteristics of the PV modules are plotted for different temperature (Figure 3) and illumination (Figure 4) conditions.

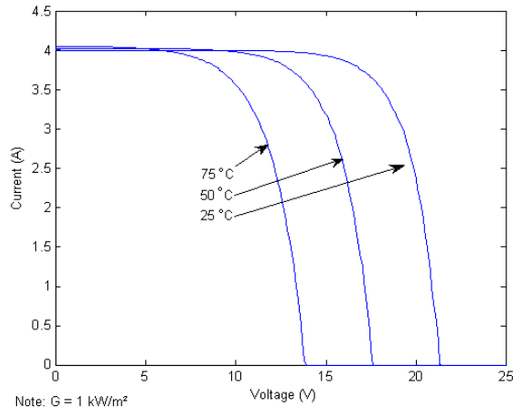

Fig. 3. PV module I-V characteristics for different temperature

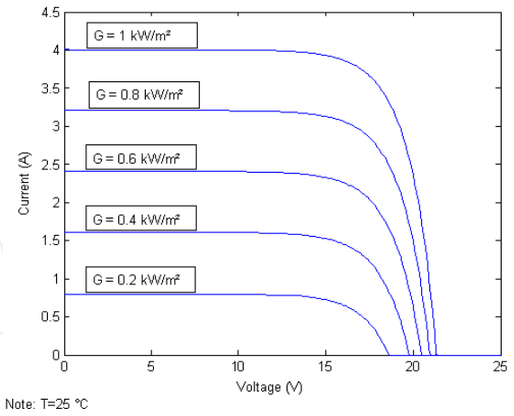

Fig. 4. PV module I-V characteristics for different illumination

2.2 Wind turbine

Some of the available power in the wind is converted by the rotor blades to mechanical power acting on the rotor shaft of the WT. The wind turbine rotor that extracts the energy from the wind and converts it into mechanical power is a complex aerodynamic system.

For state-of-the-art modelling of the rotor, blade element theory must be used. Modelling the rotor using blade element theory has, however, a number of drawbacks (Slootweg et al., 2003).

- Instead of only one wind speed signal, an array of wind speed signals has to be applied.
- Detailed information about the rotor geometry should be available.
- Computations become complicated and lengthy.

To overcome these difficulties, a simplified way of modelling the wind turbine rotor is normally used when the electrical behaviour of the system is the main point of interest. For steady-state calculations of the mechanical power from a wind turbine, the so called $C_p(\lambda, \beta)$-curve can be used. An algebraic relation between wind speed and mechanical power extracted is assumed, which is described by the well-known expression (Slootweg et al., 2003), (Cardenas & Pena, 2004):

$$P_w = \frac{1}{2}\rho\pi R^2 C_p(\lambda,\beta)v^3 \tag{10}$$

where:

P_w = power extracted from the wind (W)
ρ = air density (kg/m^3)
R = blades radius (m)
C_p = power coefficient
λ = tip speed ratio
β = pitch angle of the rotor blades (degrees)
v = wind speed (m/s)

The density ρ of air is quite low less than that of water which powers hydro plant, and this leads directly to the large size of a wind turbine. The power coefficient describes that

fraction of the power in the wind that may be converted by the turbine into mechanical work. It has a theoretical maximum value of 0.593 (the Betz limit). The power coefficient C_p of a rotor varies with the tip speed ratio λ (the ratio of rotor tip speed to free wind speed) and is only a maximum for a unique tip speed ratio. Improvements are continually being sought in the power coefficient by detailed design changes of the rotor and, by operating at variable speed; it is possible to maintain the maximum power coefficient over a range of wind speeds. However, these measures will give only a modest increase in the power output. Major increases in the output power can only be achieved by increasing the swept area of the rotor or by locating the wind turbines on sites with higher wind speeds (Burton et al., 2001).

Numerical approximations have been developed to calculate C_p for given values of λ and β (Slootweg et al., 2003), (Lei et al., 2006). For the Bergey BWC Excel 10 kVA wind turbine used at the HRI, the following equation was used to approximate the power coefficient C_p.

$$C_p = (0.0007391v^3 + 0.023649v^2 - 0.26584v + 1.2934) * (1 - 44.292\exp(-1.0762 * v)) \quad (11)$$

Figure 5 shows the wind turbine output electrical power variation with respect to wind speed.

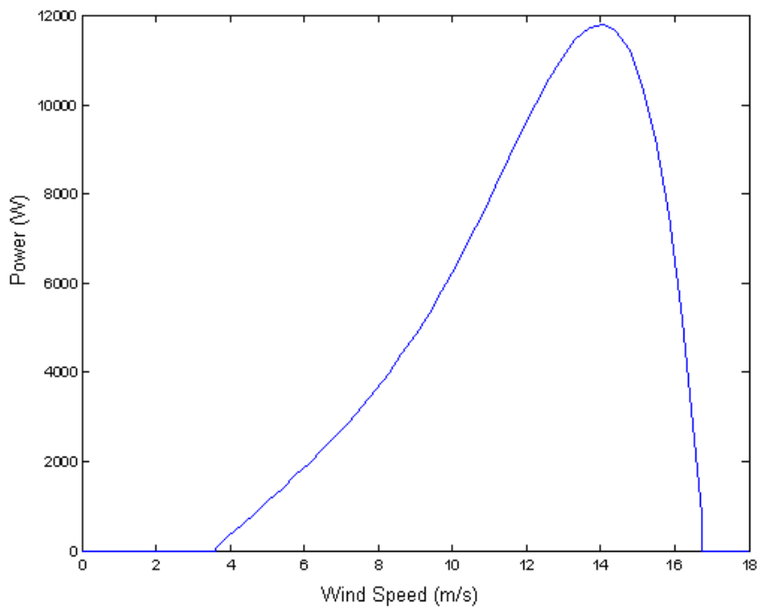

Fig. 5. Wind turbine output electrical power variation with respect to wind speed

2.3 Battery model

The battery plays the role of an energy buffer for short-term energy storage. Different models for batteries are available, in particular those suitable for electrical vehicle applications (Kélouwani et al., 2005). For stationary applications such as the renewable sources, the models described in (Vosen & Keller, 1999) use many experimental parameters that cannot be estimated easily, such as the overcharge effect (though in a properly-controlled RESHS, this effect does not happen, and hence is not included in the present

model). The main parameters which determine the battery's performance are its internal resistance, the polarization effect, and the long-term self-discharge rate. The self-discharge rate is difficult to estimate, and is itself subject to a number of factors such as the operating temperature, the number of operation cycles, and the materials and technology used in its manufacture. The battery model used in this paper presents the relation between voltage, current and the battery state of charge Q as follows (Chérif et al., 2002):
In discharge mode (I<0):

$$V(t) = V_d - g_d \frac{It}{C} + R_d I\left(1 + \frac{M_d It}{C(1 + C_d) - It}\right) \tag{12}$$

In charge mode (I>0):

$$V(t) = V_c - g_c\left(1 - \frac{It}{C}\right) + R_c I\left(1 + \frac{M_c It}{CC_c - It}\right) \tag{13}$$

where :

I = battery current (A)
V = battery voltage (V)
C = battery capacity (Ah)
T = time (h)
R = internal resistance (Ω)
g = coefficient that characterises the voltage variation ΔV = f(Q) (V)
M = slope of voltage characteristic V = f(t,I,Q)
In (12), (13), (15) and (16) the subscripts *d* and ***c*** indicate the discharging and charging modes.
The state of charge Q of the battery can be calculated through the current integral.

$$Q = \int Idt + Q_0 \tag{14}$$

where Q_0 is the initial battery charge.
In the previous equations, the term I*t can be replaced by (C-Q=Q_d), so equations (12) and (13) become

$$V(Q_d) = V_d - g_d \frac{Q_d}{C} + R_d I\left(1 + \frac{M_d Q_d}{C(1 + C_d) - Q_d}\right) \tag{15}$$

$$V(Q_c) = V_c - g_c\left(1 - \frac{Q_c}{C}\right) + R_c I\left(1 + \frac{M_c Q_c}{CC_c - Q_c}\right) \tag{16}$$

where :
Q_c=Q = cumulated charge (A.s)
Q_d = transmitted charge (during discharge) (A.s)

2.4 Electrolyzer model

Electrolyzers operate in either current mode or voltage mode. When they are run in voltage mode, voltage is applied to the electrolyzer and, depending on the operating conditions, the electrolyzer draws the current from the source. After a couple of transient cycles it has reached its steady state value. However, most of the commercially available electrolyzers run in current mode, with a polarization characteristic as shown in Figure 6. This characteristic can be represented as a sum of linear, logarithmic and exponential functions.

$$V = E_0(T) + R(T) * I + b(T) * ln(I) + m(T) * exp(n * I) \quad (17)$$

where :

E_o = Reversible potential
I = current (A)
T = temperature (°C)
b, m, R = coefficients that depend on temperature
n = constant

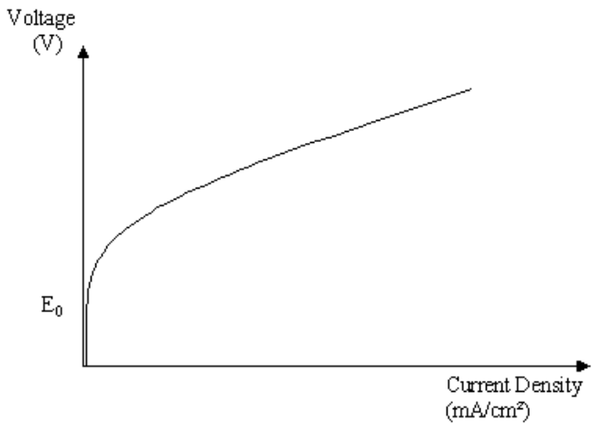

Fig. 6. Electrolyzer polarisation characteristic

Real coefficients were obtained from experimental data for a Stuart electrolyzer. Two series of data at two temperatures (23.5°C and 53°C) and one series with fixed voltage were used. The curves are extrapolated in temperature by modifying eq. 17 (assuming its exponential term can be ignored):

$$V = E_0 + RI + b\,ln(I) \quad (18)$$

By varying the resistance R one can optimize the equation $E_0 + b\,ln(I)$ for the curves at temperatures 23.67°C and 53.51°C via the correlation coefficient. Then the coefficients thus determined: E_0, b and R are extrapolated linearly in temperature. Figure 7 shows several of these polarisation curves, as well as certain points taken from the series of data with fixed voltage.

$$V = E_0 + RI + b\,ln(I) + (0.1716\,exp(-0.0612T)) * exp(0.055I) \quad (19)$$

where :

$E_0(T) = 32.5628 - 0.00677*T$
$R(T) = 0.0002089*T + 0.00955$
$b(T) = 3.374 - 0.0194*T$

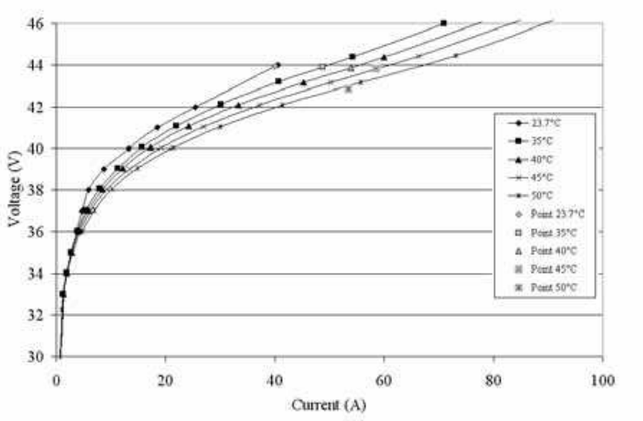

Fig. 7. Stuart electrolyzer polarisation curve

2.5 Fuel cell model

Depending on the current drawn, the fuel cell converts hydrogen and thereby produces voltage as a function of current. The equations used depend on the empirical form of the fuel cell model (Doumbia et al., 2007). The polarisation curve of the fuel cell (Figure 8) can be divided into three regions: the activation overvoltage region, the ohmic overvoltage region, and the thermodynamic overvoltage region. This curve can be represented (again, as in the electrolyzer model) by a sum of linear, logarithmic and exponential functions:

$$V = E_0 - b(T) * ln(I) - R(T) * I - m(T) * exp(n * I) \quad (20)$$

where :
I = current (A)
T = temperature (°C)
b, R, m = coefficients that depend on the temperature
n = constant
Table 1 summarizes the coefficients values of the Ballard MK5-E fuel cell used at the IRH.

Coefficients	Values
E_0 (V)	1.05
b (V)	$4.01 \times 10^{-2} - 1.40 \times 10^{-4}T$
R (kΩ cm²)	$4.77 \times 10^{-4} - 3.32 \times 10^{-6}T$
m (V) : T ≥ 39°C	$1.1 \times 10^{-4} - 1.2 \times 10^{-6}T$
m (V) : T < 39°C	$3.3 \times 10^{-3} - 8.2 \times 10^{-5}(T-39)$
n	8.0×10^{-3}

Table 1. Ballard MK5-E fuel cell coefficients values

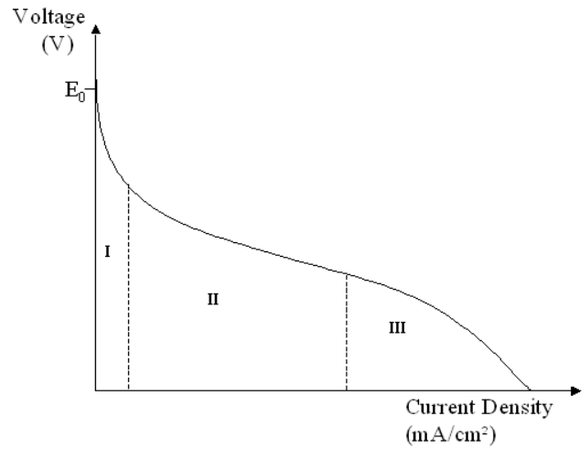

Fig. 8. Fuel cell polarisation curve

The commands for the electrolyzer and for the fuel cell are taken from the equation for the reference current. The form of this equation depends on the power demand and on the temperature of the electrolyzer. To validate system simulation model, the control system is designed in such a way that if the state-of-charge (SOC) exceeds 55%, then the electrolyzer kicks in (i.e. the excess energy is converted to stocked hydrogen), while if the OSC is less than 45%, the extra energy needed is drawn from the hydrogen by activating the fuel cell.

3. Integrated system simulation results

The global renewable energy system with hydrogen storage (RESHS) was modelled and simulated using Matlab/Simulink™ and Labview softwares. The simulation model includes sub-systems for the photovoltaic array, wind power generator, the electrolyzer and the fuel cell. The currents from the photovoltaic array and wind generator are sent to the DC bus which feeds the batteries. The current consumed by the load and the electrolyzer is withdrawn from the DC bus.
For validation purpose, the HRI RESHS was simulated using the state-of-charge (SOC) control strategy. The control system verifies the state of charge of the batteries and sends control signals to the electrolyzer or the fuel cell via DC/DC converters. When the state-of-charge of the batteries is high, the control unit activates the electrolyzer by sending a control signal to the buck converter (to decrease the energy level). The excess energy is thus converted into hydrogen which is stored for latter use. On the other hand, when the state of charge of the batteries is low, the control unit activates the fuel cell via the boost converter. The stored hydrogen is then converted to electrical energy which is sent to the DC bus to supply local loads.

The Figure9 shows the Matlab/Simulink model of the RESHS. This global model integrates the model of all the system sub-units (PV, wind, electrolyzer, fuel cell, batteries). The behaviour of the system is simulated for six-day periods in the months of January

(winter time) and July (summer time). The voltage, currents, power of all sub-units can be monitored and plotted. For simulation test purpose, the system is controlled such as if the state of charge of the batteries is too high or too low, respectively the electrolyzer or the fuel cell is started to reduce or increase the energy stocked in the batteries. Input data such as illumination, temperature, wind's speed and load consumption are imported from corresponding sub-systems.

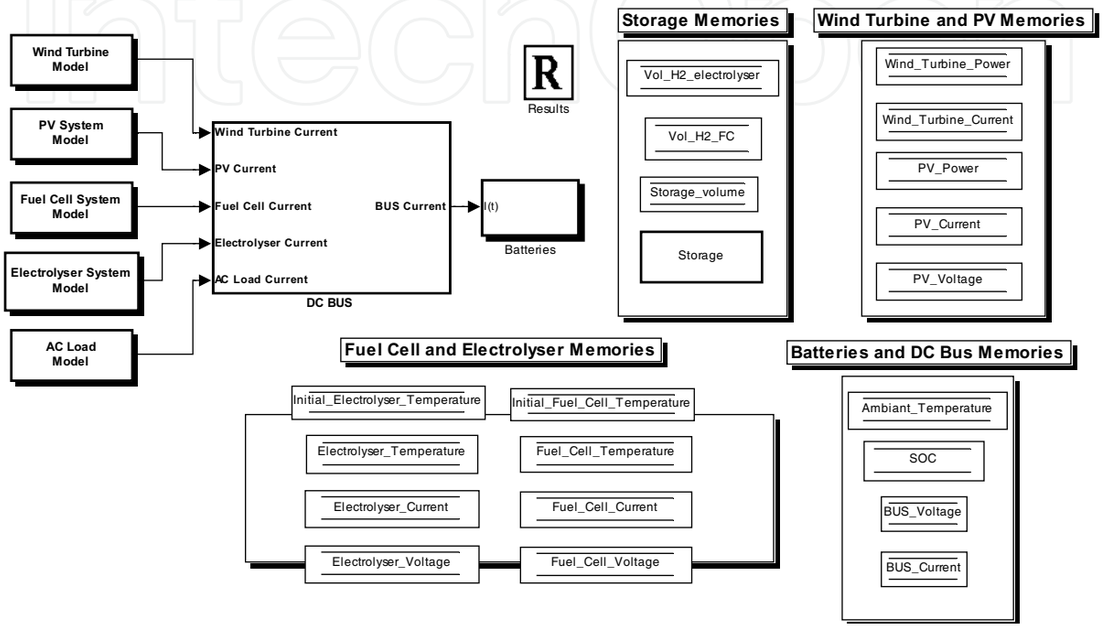

Fig. 9. Matlab/Simulink simulation model of the renewable energy system

Figure 10 and Figure 14 show the input data of temperature, illuminance and wind speed respectively for January and July. With these meteorological input conditions, the resulting photovoltaic and wind powers are shown in Figure 11 and Figure 15. The peaks of power produced by the wind generator can be seen reflected in the total DC bus currents (Figure 12 and Figure 16). The state of charge and the powers of the electrolyzer and of the fuel cell are shown in Figure 13 and Figure 17. These last two figures clearly show the correlation between the state of charge of the batteries and the activation of the electrolyzer (when SOC > 55%) or of the fuel cell (when SOC < 45%).

These simulation results are confirmed using both modelling and simulation softwares Matlab/ Simulink™ (Doumbia et al., 2009) and Labview (Doumbia et al., 2009).

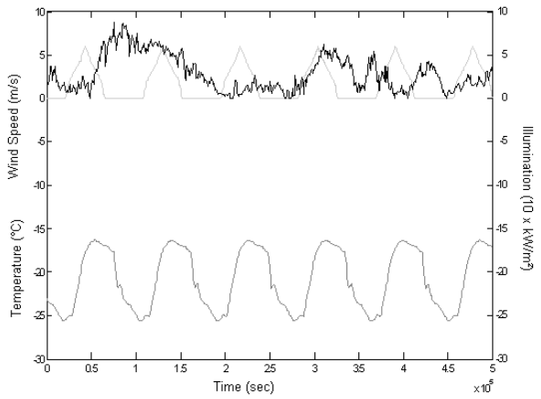

Fig. 10. Wind speed, temperature and illumination in January

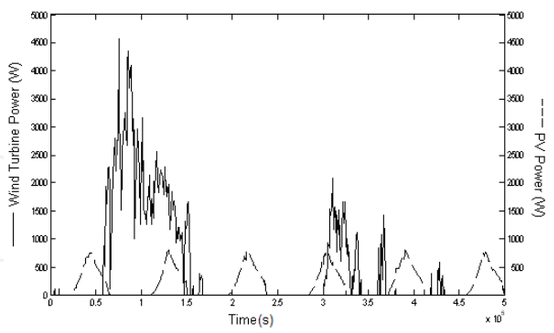

Fig. 11. Wind turbine and photovoltaic array power in January

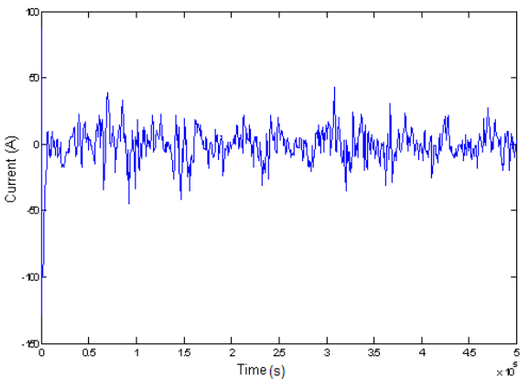

Fig. 12. DC bus current in January

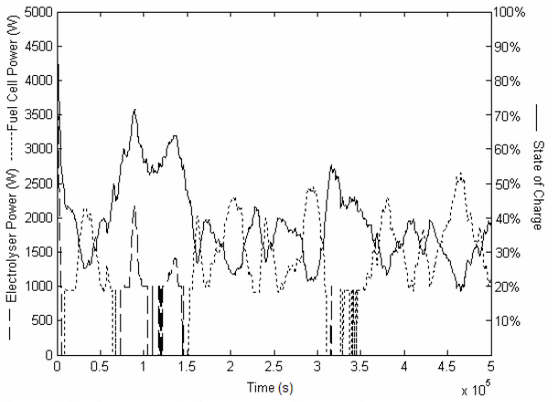

Fig. 13. State of charge, electrolyzer power and fuel cell power in January

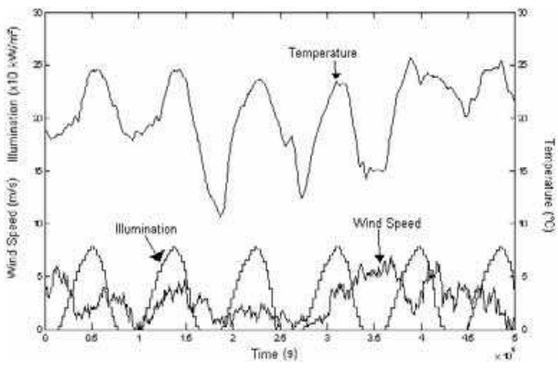

Fig. 14. Wind speed, temperature and illumination in July

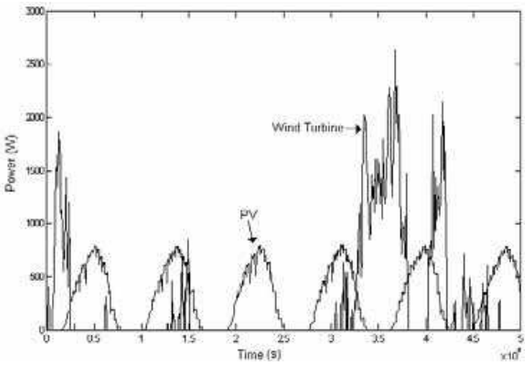

Fig. 15. Wind turbine and photovoltaic array power in July

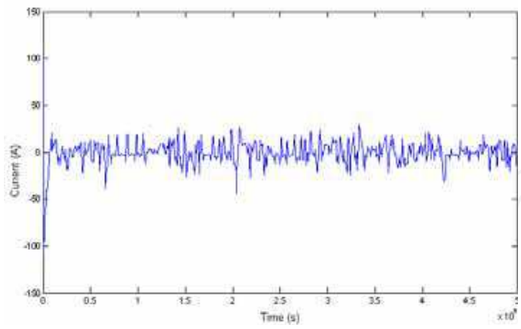

Fig. 16. DC bus current in July

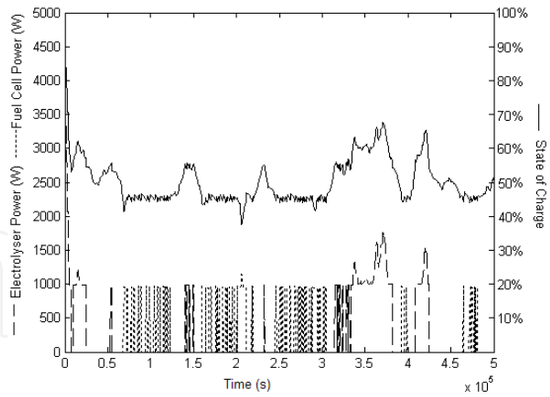

Fig. 17. State of charge, electrolyzer power and fuel cell power in July

4. Experimental study

4.1 Operation in stand-alone mode

The Hydrogen Research Institute's RESHS was investigated experimentally for stand-alone operation (Kodjo et al., 2004). The energy available from the WTG and the PV array are shown respectively in Figure 18 and Figure 19. The limits of energy levels in the control algorithm were set to start the electrolyzer at 99% of energy level at the DC bus or above and to stop the electrolyser at 84%. The fuel cell on and off operations was set to 83% and 85%, respectively. During this operation, the electrolyzer input power and the fuel cell output power are shown in Figure 20, the load profile and the batteries charging/discharging power are shown in Figure 21. The system started its operation at 9:20 AM, when the batteries energy level was at 100% SOC. It has been observed that the power supplied to the electrolyzer is mainly come from the short-term energy storage (batteries) due to the non-availability of sufficient energy from the RE sources during the operation. The power flow of the batteries (charging/discharging) was also carefully monitored. The electrolyzer and the fuel cell operations were started and stopped automatically, when the energy levels at DC bus have reached to the pre-defined levels of the control algorithm.

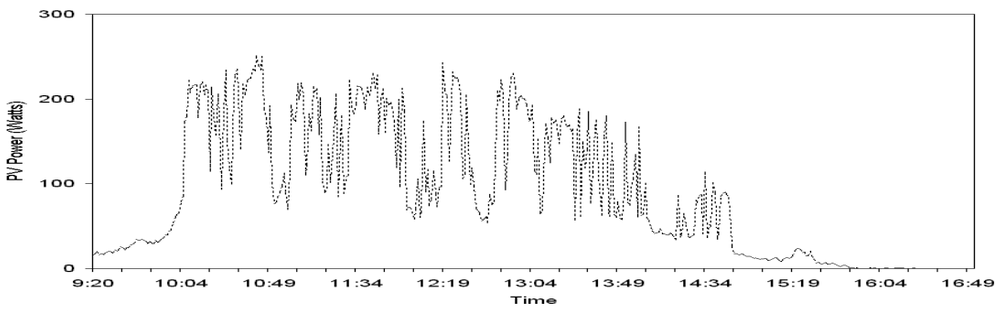

Fig. 18. Photovoltaic power

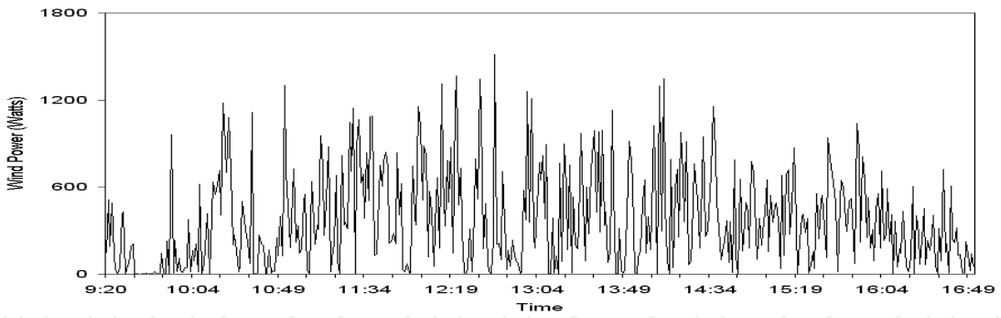

Fig. 19. Wind power

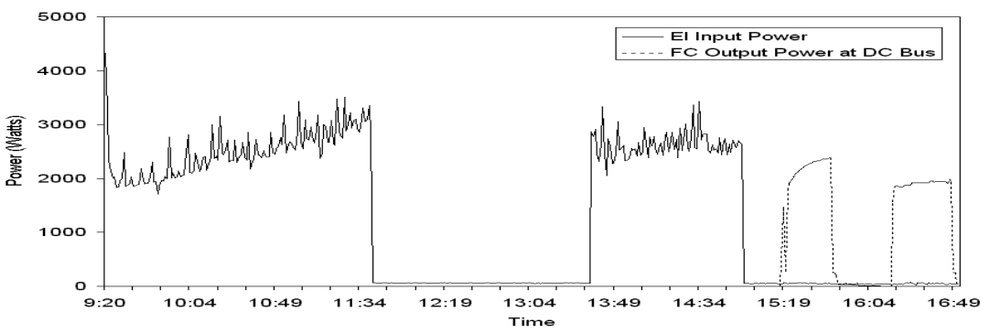

Fig. 20. Electrolyzer and fuel cell powers

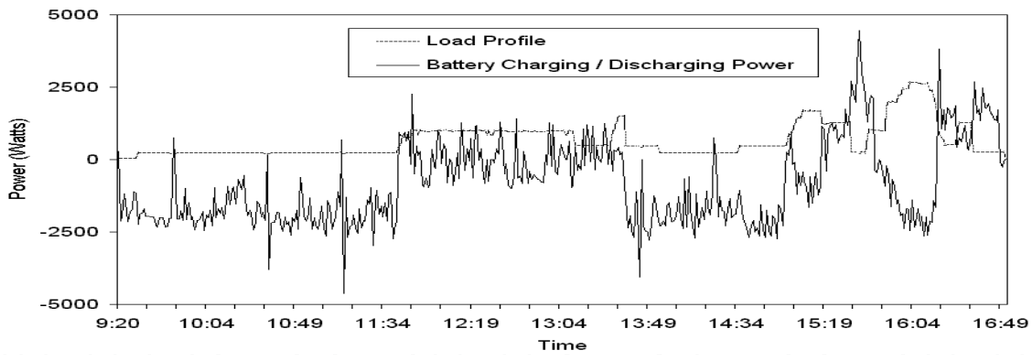

Fig. 21. Load and batteries powers

4.2 Operation in grid-connected mode

The HRI renewable energy system was investigated also in grid-connected operation mode (Figure 22). When connected to the utility grid, the interconnecting power electronic interface (a Trace Engineering SW4458 inverter) can be operated in four modes: Float, Silent, Sell and Low Battery Transfer.

Fig. 22. Grid-connected renewable energy system with hydrogen storage

Operation in Float mode

The Float mode maintains the batteries at the float voltage level. This can be used when the source of power is a utility grid or a generator. When alternating current (AC) power is available, the inverter completes a full three-stage charge cycle and then holds the battery at the float level until the source of utility power is no longer available. This setting is appropriate for use with stand-alone systems with back-up generators or utility back-up systems. If photovoltaic or wind power is available and the battery is full, the excess power will be used to directly power the AC loads connected to the inverter output (Trace Engineering, 1999).

The Float mode was used to operate the RES from 11:55 to 16:38 (April 30, 2009). Figure 23 shows the system's operating characteristics. In the Float mode, the load (Figure 20a) is feed by batteries (Figure 23d) as long as the DC bus voltage (Figure 23f) is greater than a pre-defined threshold minimum (Low Battery Transfer Voltage) set to 47V in our case. When the DC bus voltage falls under 47V, the utility grid begins to feed the loads and batteries are recharged by the energy (if available) coming from solar panels (Figure 23g) and from the wind turbine generator (Figure 23h). The utility grid continues to power the loads as long as the DC bus voltage does not reach another pre-defined voltage level (Low Battery Cut In voltage), set to 52V (Figure 23c) in during this test. Figure 23b and Figure 23e show respectively the batteries current and state of charge variation.

Operation in Silent mode

This mode does not maintain the battery at float voltage all the time. The inverter performs a bulk charge (i.e. charging at a preset voltage level) of the batteries once per day, from the utility grid. The inverter then goes totally silent and will wait for the utility grid to fail, or until the next day when it performs another bulk charge. This mode is typically used in utility back-up applications (Trace Engineering, 1999).

The SER was tested in this mode on April 20th, 2009 from 12:00 to 16:15. The load was composed of the electrolyzer (400W) and lighting (380W) (Figure 24a). At the beginning of the test, the inverter was in bulk charge mode until 12:45 (Figure 24c). During this period, the utility network recharges batteries (Figure 24b, Figure 24d) by maintaining the batteries voltage at 53.6V (Figure 24f). After the Bulk charge period, the inverter works in Silent mode. Then, the DC bus voltage depends on the power balance between the input powers (photovoltaic power Figure 24g; and wind power Figure 24h) and output powers (electrolyzer and lighting).

Operation in Sell mode

SELL mode enables the inverter to send the excess power to the grid. This mode must have the approval of the local power utility prior to its use. In this mode, when power from photovoltaic array or wind generator is available, it will be used to power any AC load connected to the AC output of the inverter. Any excess power available from the system will be sold "into" the utility grid (Trace Engineering, 1999).

The SER was tested in this mode on May 5th, 2009 from 12:00 to 16:30 (Figure 25). A 460W local AC load (Figure 25a) was connected to the inverter output. The inverter was programmed to send up to 7A (800VA supplementary power) to the utility grid if the DC bus voltage is higher than a pre-defined threshold voltage (48V). At the beginning of the test, as the DC bus voltage (Figure 25f) is higher than the pre-defined sell voltage, the loads are powered by batteries (Figure 25d) through the inverter; this leads to the batteries discharging (Figure 25e). When renewable PV (Figure 25g) and wind (Figure 25h) energy sources are available, the power provided by the batteries (inverter) is reduced. When the DC bus voltage reaches the pre-defined 48V, the energy from the batteries is reduced (Figure 25b, Figure 25c) and loads are mainly powered by the utility grid and renewable energy sources.

Operation in Low battery transfer mode

The Low battery transfer mode allows a system to switch automatically between utility connected and stand alone battery operation. In this mode, the inverter will power the loads from the battery and other energy sources until the battery voltage drops to the pre-defined "low battery transfer voltage" value. It will then connect to the utility grid and charge the battery. The loads will be powered by the utility until the battery voltage reaches the "Low battery cut in voltage" value. The inverter will then disconnect the utility and power the loads from the battery or any other connected DC power source. This mode is often used instead of the Sell mode because approval from the utility is not required - no power will be sent into the utility distribution system when this mode is selected (Trace Engineering, 1999).

The SER was tested in Low battery transfer mode on May 11th, 2009 from 11:45 to 16:33 (Figure 26). Around 1200W local AC load (Figure 26a) was connected to the inverter output. At the beginning of the test, as the DC bus voltage (Figure 26f) is higher than the pre-defined threshold voltage (47V), the loads are powered by batteries (Figure 23b, Figure 26d) through the inverter; this leads to the batteries discharging (Figure 26e). When the DC bus voltage reaches the pre-defined 47V, the utility grid begins to power the local load (Figure 26c). At all time, if renewable PV (Figure 26g) or wind (Figure 26h) energy source is available, the power provided by the batteries or by the utility grid is reduced.

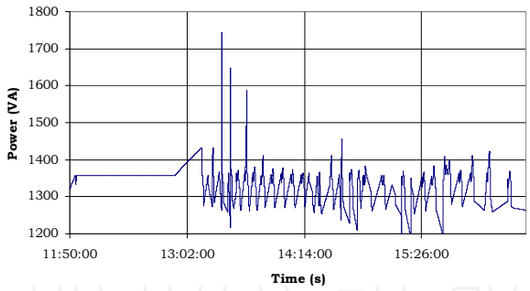

a) Local Load power

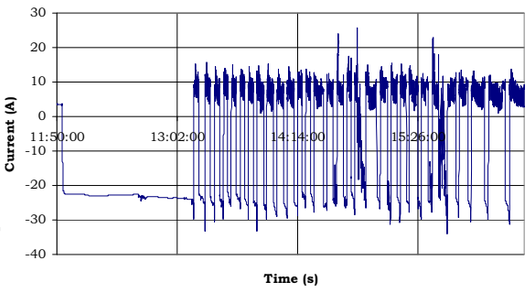

b) Batteries current

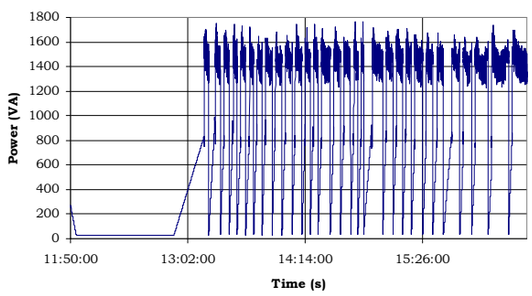

c) Inverter power

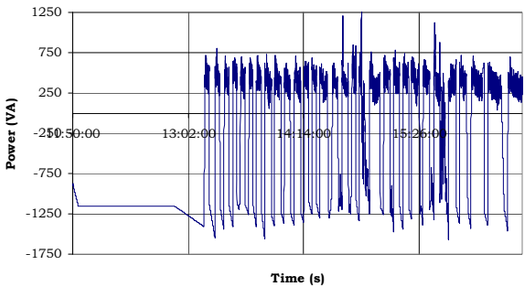

d) Batteries power

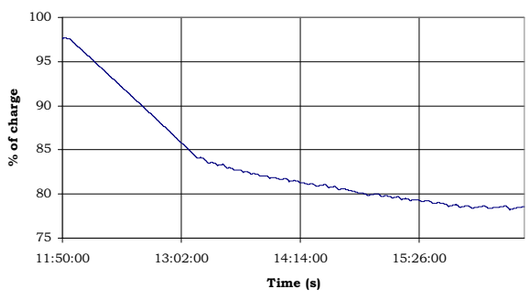

e) State of charge

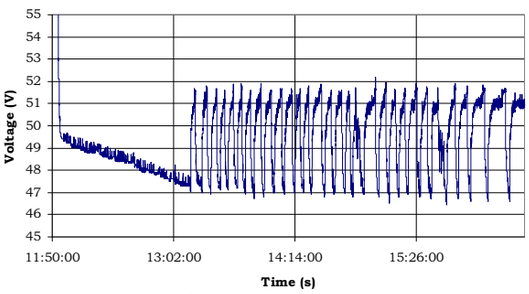

f) DC bus voltage

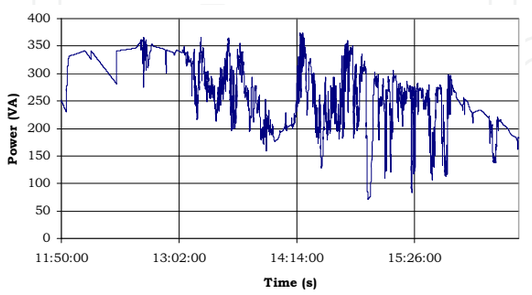

g) Photovoltaic power

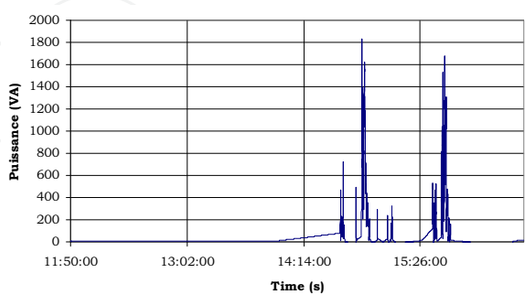

h) Wind power

Fig. 23. Grid-Connected RES operation in Float mode

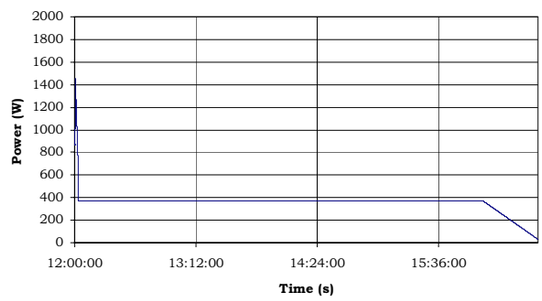

a) Electrolyzer power

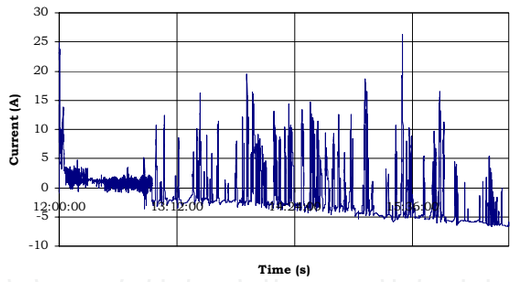

b) Batteries current

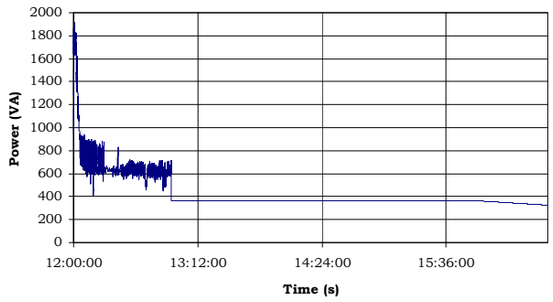

c) Inverter power

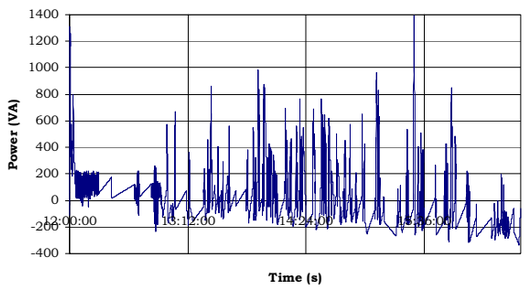

d) Batteries power

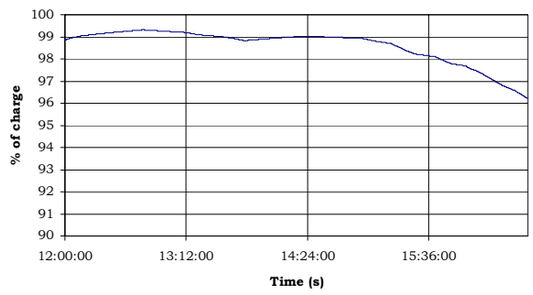

e) State of charge

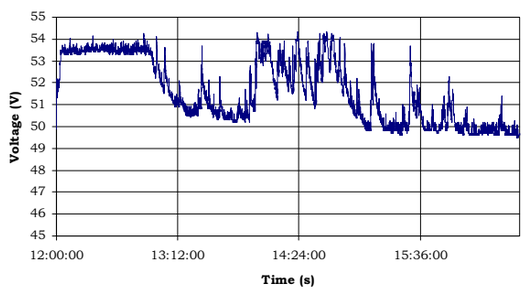

f) DC bus voltage

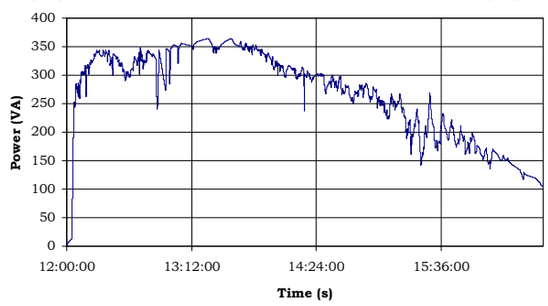

g) Photovoltaic power

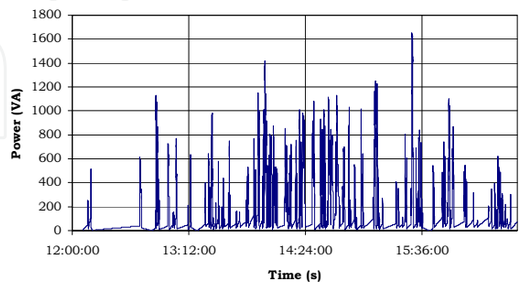

h) Wind power

Fig. 24. Grid-Connected RESHS operation in Silent mode

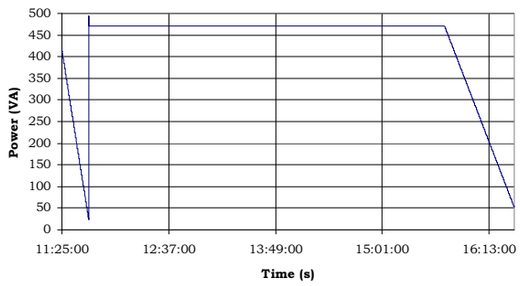

a) Local load power

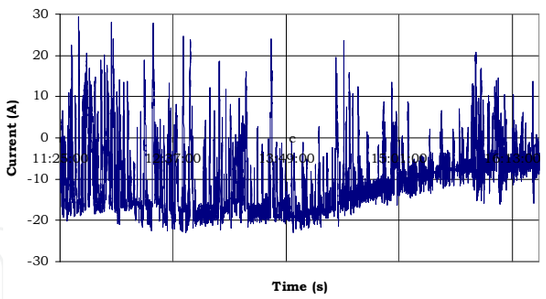

b) Batteries current

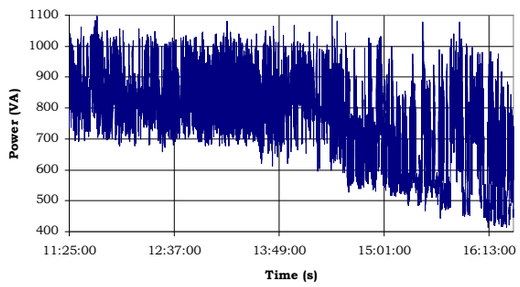

c) Inverter sell power

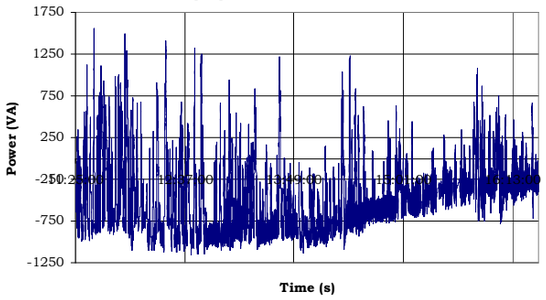

d) Batteries power

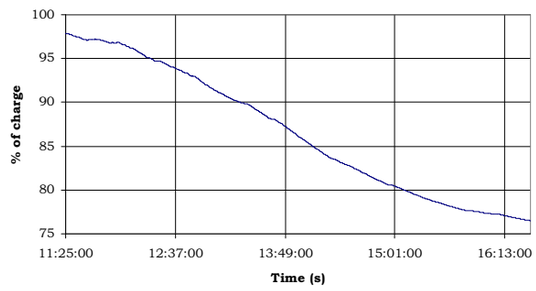

e) State of charge

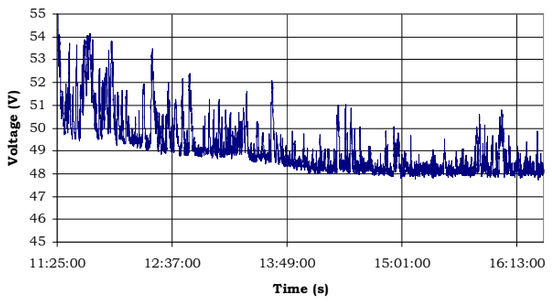

f) DC bus voltage

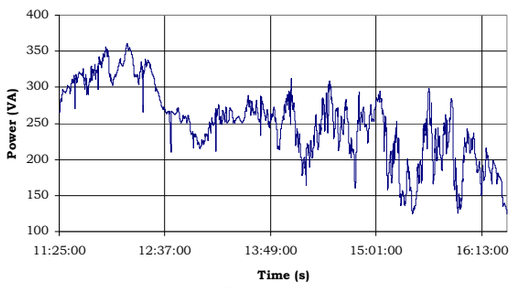

g) PV power

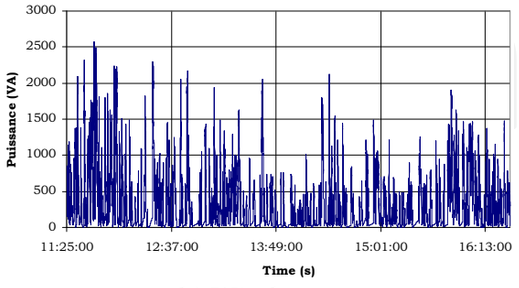

h) Wind power

Fig. 25. Grid-Connected RESHS operation in Sell mode

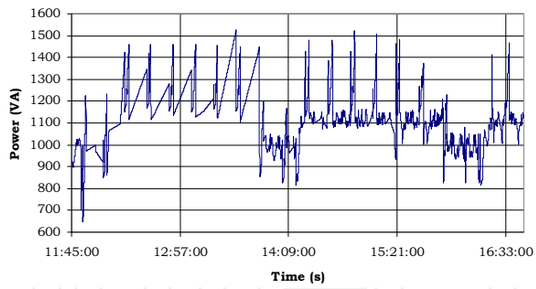

a) Local load power

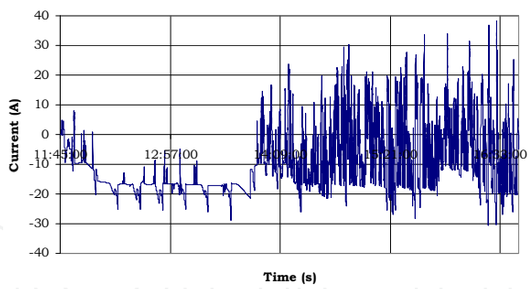

b) DC bus current

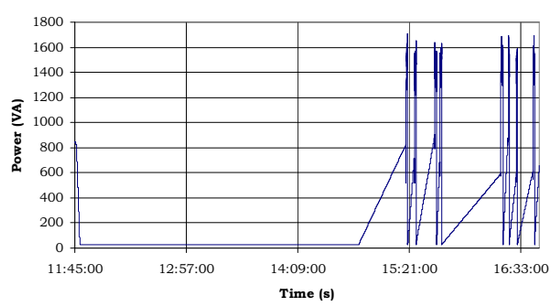

c) Utility grid power

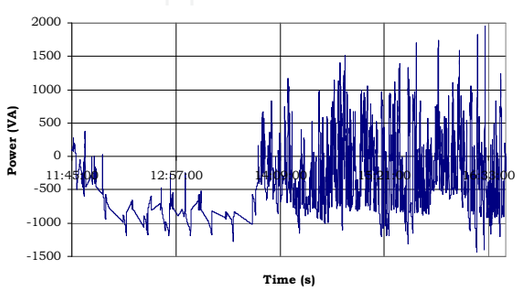

d) Batteries power

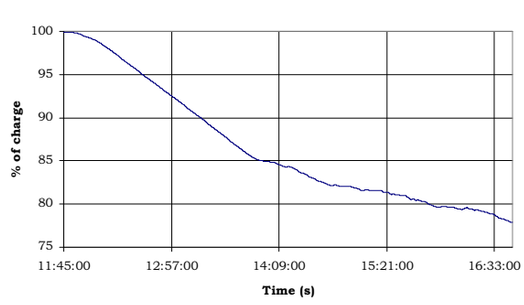

e) State of charge

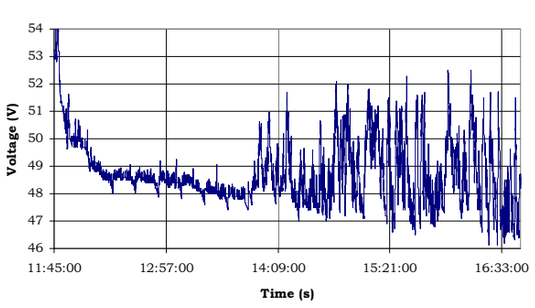

f) DC bus voltage

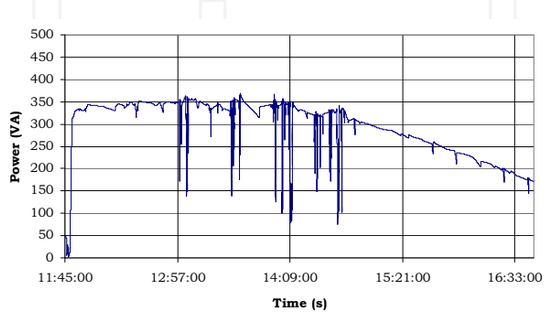

g) PV power

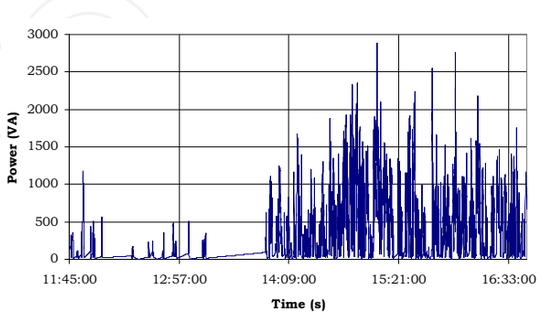

h) Wind power

Fig. 26. Grid-Connected RESHS operation in Low battery transfer mode

5. Conclusion

This paper presents the modelling, simulation and experimental study of a renewable energy system with hydrogen storage (RESHS). Solar photovoltaic array, wind generator, electrolyzer, fuel cell and batteries modelling principles are presented. Matlab/Simulink and Labview programming tools were used for modelling and simulation purpose. The models of the main components have been developed and integrated into the whole system in order to study its general performance. The RESHS was investigated experimentally in stand-alone and grid-connected operation modes. For different grid-connected operating modes (Float, Silent, Sell, Low battery transfer), the system's operating conditions were monitored and power transfer was analyzed. The renewable energy system has shown satisfactory performances for operation with short term (battery) and long-term (hydrogen) energy storage. However, a control strategy based on the state of charge (SOC) of the batteries needs to be developed to improve the performances of the RESHS in grid-connected operation mode.

6. Acknowledgement

This work has been supported by the LTE Hydro-Québec and the Natural Sciences and Engineering Research Council of Canada.

7. References

Agbossou K., Kolhe M., Hamelin J., and Bose T. K. (2004). Performance of a Stand-Alone Renewable Energy System Based on Energy Storage as Hydrogen, *IEEE Transactions on Energy Conversion,* Vol. 19, No. 3, Page(s): 633-640, September 2004.

Burton T., Sharpe D., Jenkins N. and Bossanyi E. (2001). *Wind Energy Handbook*, John Wiley & Sons, LT, 2001.

Cardenas R., R. Pena (2004). Sensorless Vector Control of Induction Machines for Variable-Speed Wind Energy Applications, *IEEE Trans. On Energy Conversion*, Vol. 19, No. 1, Page(s): 196 - 205, March 2004.

Chérif A., Jraidi M. and Dhouib A (2002). A battery ageing model used in stand alone PV systems, *Journal of Power Sources*, vol.112, Issue 1, Page(s): 49-53, 2002.

Doumbia, M.L., Agbossou, A., Granger, E. (2007). Simulink Modelling and Simulation of a Hydrogen Based Photovoltaic/Wind Energy System, *Eurocon* The *International Conference on "Computer as Tools"*, Page(s): 2067 – 2072, Warsaw, September 2007.

Doumbia, M.L., Agbossou, A., Proulx, C-L. (2009). Labview Modelling and Simulation of a Hydrogen Based Photovoltaic/Wind Energy System, *Electromotion,* 8th International Symposium on Advanced Electromechanical Motion Systems, Lille, July 2009, France.

Gow J. A., Manning C.D. (1999). Development of a photovoltaic array model for use in power-electronics simulation studies, *IEE Proc.-Electr. Power Appl.*, Vol. 146, No. 2, March 1999.

Kélouwani S., Agbossou K., and Chahine R. (2005). Model for Energy Conversion in Renewable Energy System with Hydrogen Storage, *Journal of Power Sources*, vol. 140, no 2, p. 392-399, 2005.

Lei Y., Mullane A., Lightbody G., and Yacamini R. (2006). Modelling of the Wind Turbine with a Doubly Fed Induction Generator for Grid Integration Studies, *IEEE Trans. On Energy Conversion*, Vol. 21, No. 1, Page(s): 257 - 264, March 2006.

Kim S-L., Jeon J-H., Cho C-H., Ahn J-B. and Kwon S-H. , (2008). Dynamic Modeling and Control of a Grid-Connected Hybrid Generation System With Versatile Power Transfer. *IEEE Trans. On Industrial Electronics,* Vol. 55 No. 4, April 2008.

Slootweg J. G., De Haan S., Polinder H., and Kling W. (2003). General Model for Representing Variable Speed Wind Turbines in Power System Dynamics Simulations. *IEEE Trans. On Power Systems*, Vol. 18, No. 1, February 2003.

Trace Engineering (Xantrex), *SW Series Inverter/Chargers Owner's Manual*, 1999.

Vosen S.R., Keller J.O. (1999). Hybrid energy storage systems for stand-alone electric power tems: optimization of system performance and cost through control strategies. *International Journal of Hydrogen Energy*, Vol. 24, Page(s): 1139-1156, 1999.

Walker, G. (2000). Evaluating MPPT Converter Topologies Using a MatLab PV Model, *Journal of Electrical & Electronics Engineering*, vol. 21, no 1**,** pp. 49 – 56, Australia, 2000.

Renewable Energy
Edited by T J Hammons

ISBN 978-953-7619-52-7
Hard cover, 580 pages
Publisher InTech
Published online 01, December, 2009
Published in print edition December, 2009

Renewable Energy is energy generated from natural resources-such as sunlight, wind, rain, tides and geothermal heat-which are naturally replenished. In 2008, about 18% of global final energy consumption came from renewables, with 13% coming from traditional biomass, such as wood burning. Hydroelectricity was the next largest renewable source, providing 3% (15% of global electricity generation), followed by solar hot water/heating, which contributed with 1.3%. Modern technologies, such as geothermal energy, wind power, solar power, and ocean energy together provided some 0.8% of final energy consumption. The book provides a forum for dissemination and exchange of up-to-date scientific information on theoretical, generic and applied areas of knowledge. The topics deal with new devices and circuits for energy systems, photovoltaic and solar thermal, wind energy systems, tidal and wave energy, fuel cell systems, bio energy and geo-energy, sustainable energy resources and systems, energy storage systems, energy market management and economics, off-grid isolated energy systems, energy in transportation systems, energy resources for portable electronics, intelligent energy power transmission, distribution and inter-connectors, energy efficient utilization, environmental issues, energy harvesting, nanotechnology in energy, policy issues on renewable energy, building design, power electronics in energy conversion, new materials for energy resources, and RF and magnetic field energy devices.

How to reference
In order to correctly reference this scholarly work, feel free to copy and paste the following:

Mamadou Lamine Doumbia and Kodjo Agbossou (2009). Photovoltaic/Wind Energy System with Hydrogen Storage, Renewable Energy, T J Hammons (Ed.), ISBN: 978-953-7619-52-7, InTech, Available from: http://www.intechopen.com/books/renewable-energy/photovoltaic-wind-energy-system-with-hydrogen-storage

INTECH
open science | open minds

InTech Europe
University Campus STeP Ri
Slavka Krautzeka 83/A
51000 Rijeka, Croatia
Phone: +385 (51) 770 447
Fax: +385 (51) 686 166
www.intechopen.com

InTech China
Unit 405, Office Block, Hotel Equatorial Shanghai
No.65, Yan An Road (West), Shanghai, 200040, China
中国上海市延安西路65号上海国际贵都大饭店办公楼405单元
Phone: +86-21-62489820
Fax: +86-21-62489821

IntechOpen